Inorganic Chemistry

Article

pubs.acs.org/IC

Fe_3O_4 Nanocrystals Tune the Magnetic Regime of the Fe/Ni Molecular Magnet: A New Class of Magnetic Superstructures

Giorgio Zoppellaro,[†] Jiří Tuček,[†] Radovan Herchel,[‡] Klára Šafářová,[†] and Radek Zbořil*[,†]

[†]Regional Centre of Advanced Technologies and Materials, Departments of Physical Chemistry and Experimental Physics, Faculty of Science, Palacky University, 17. listopadu 1192/12, 771 46 Olomouc, Czech Republic

[‡]Department of Inorganic Chemistry, Faculty of Science, Palacky University, 17. listopadu 1192/12, 771 46 Olomouc, Czech Republic

Supporting Information

ABSTRACT: A new class of organometallic−inorganic magnetic material was engineered by a sonochemically assisted self-assembly process between magnetite nanoparticles (biogenic Fe_3O_4, hard constituent) functionalized with isonicotinic acid and a metamagnetic organometallic complex ($[Ni(en)_2]_3[Fe(CN)_6]_2{\cdot}3H_2O$, soft constituent). In such bottom-up methodology, hard and soft counterparts form well-organized microdimensional clusters that showed morphological fingerprints and magnetic behavior clearly distinct from those of the initial building units. In the engineered soft−hard material, the magnetite nanocrystals induced ferromagnetic ordering at room temperature of closer contact layers of $[Ni(en)_2]_3[Fe(CN)_6]_2{\cdot}3H_2O$, thus demonstrating the ability to sensibly modify the $[Ni(en)_2]_3[Fe(CN)_6]_2{\cdot}3H_2O$ paramagnetic regime. The magnetic ordering of $[Ni(en)_2]_3[Fe(CN)_6]_2{\cdot}3H_2O$ was triggered by the intrinsic local field of the hard magnetic nanocrystals, which resembled, to some extent, the effects promoted by large, external magnetic fields.

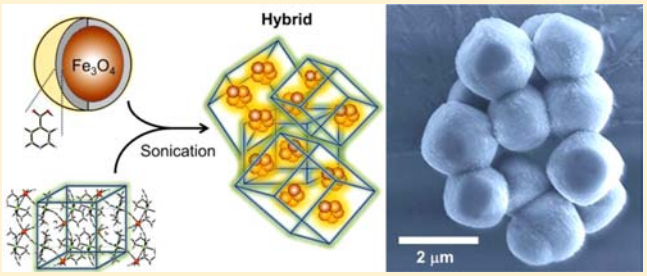

INTRODUCTION

The design and synthesis of core−shell iron oxide nanoparticles (FeNPs), mainly based on naturally occurring magnetite (Fe_3O_4) or maghemite (γ-Fe_2O_3) cores, have been fascinating topics of research for chemists and physicists for almost two decades.[1] Depending on the shell composition, these magnetic systems can become functional units in storage information devices, sensors, probes, contrast agents (magnetic resonance imaging), drug carriers, anticancer agents, and photocatalysis.[2−6] Functionalization of the nanoparticle's surface is generally obtained by organic, organometallic, and/or inorganic coating materials.[7−11] FeNPs that merge the ferromagnetic magnetite/maghemite core (FM) with an antiferromagnetic shell (AFM), usually composed of FeO layers, and those containing inverted architectures deliver model materials sensitive to changes in the magnetic ordering at the AFM/FM interface, a characteristic suitable for exploitation in the field of spintronics.[12−19] FeNPs functionalized with organic molecules containing hydrophilic substituents are envisioned to operate mainly in biological environments.[20] After the organic coating architecture has been selected, the nanoparticle systems can act as sensors, exhibit loading ability of chemotherapeutics (e.g., doxorubicin), or operate as contrast agents in medical diagnostics.[21−28] In particular, the establishment of noncovalent interactions between the organic shell and the drug is an important functional characteristic for the nanoparticle that acts as nanocarrier because it prevents chemical modification of the pharmaceutically active component during the transport process.[20] Such an approach to the synthesis in this category of functional FeNPs takes inspiration directly from many of the processes occurring in nature, where highly organized molecular assemblies and more sophisticated functions (e.g., the genetic information stored in the DNA) can emerge from the combination of distinct building units held together by weak interactions, for example, electrostatic forces, H-bonding, and $\pi-\pi$ stacking. While the self-assembly event is well-recognized as an effective path in which evolution acts in nature, the direct application of this strategy on the chemical bench for the synthesis of nanostructured materials is difficult to accomplish, especially when a precise set of chemical/physical properties is envisioned beforehand.[29] The synthesis of soft−hard magnetic systems based on the noncovalent self-assembly process of diverse units is by far less explored compared to that of soft−hard magnetic hybrids obtained via cold-pressed mixtures of various metal oxides.[30−34]

In this work, we report the synthesis and detailed physical properties of a magnetic system composed of soft−hard components which was obtained following the noncovalent approach and the self-assembly pathway in solution. As shown in Figure 1, a hybrid material (micrometer-sized, termed hereafter hybrid) emerged from the combination of magnetite nanoparticles (FeNPs, hard component) surface functionalized with isonicotinic acid and a metamagnetic molecule [Ni-

Received: April 8, 2013
Published: June 24, 2013

   dx.doi.org/10.1021/ic4008729 | *Inorg. Chem.* 2013, 52, 8144−8150

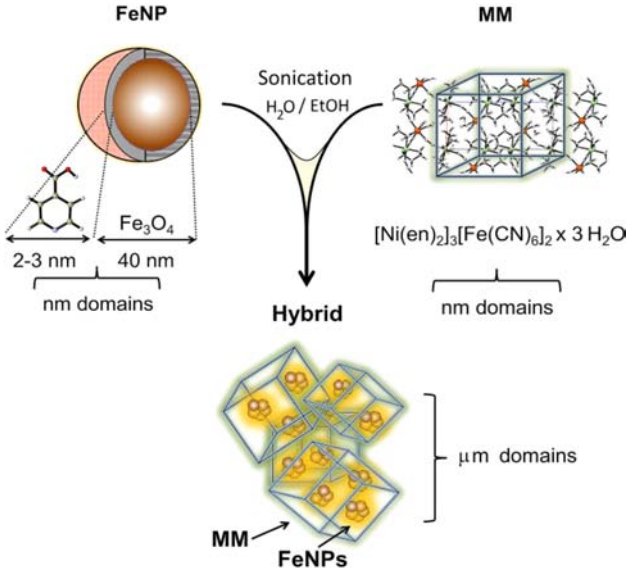

Figure 1. Schematic representation of the sonication-assisted self-assembly event that merged the two spin active components, FeNP functionalized with isonicotinic acid and MM, in the morphologically new entity, the hybrid system.

$(en)_2]_3[Fe(CN)_6]_2 \cdot 3H_2O$ (termed hereafter MM, soft component). The hybrid system displayed morphological fingerprints clearly distinct from those present in FeNPs and MM as isolated systems. Most notably, it also exhibited magnetic properties different than those expected from the pure FeNPs and MM average. In the hybrid material, a strong modification of the magnetic regime of MM occurred in response to the local magnetic field generated by the FeNPs; hence, such a noncovalent approach demonstrated the possibility of using a strong intrinsic field generated by one spin active component as a field tuner for the second component.

EXPERIMENTAL SECTION

Chemicals. All of the starting chemicals were of analytical reagent grade and have been used as received. The $[Ni(en)_3]Cl_2 \cdot 2H_2O$ precursor was prepared according to the literature procedure,[35] and the magnetite (Fe_3O_4) nanoparticles (NPs) were obtained from magnetosomes and purified as previously reported.[36]

Synthesis of the Core–Shell FeNPs. Biogenic Fe_3O_4 nanoparticles (120 mg, 0.52 mmol) were suspended in deionized water (50 mL), and the solution was degassed by nitrogen bubbling. Separately, isonicotinic acid (120 mg, 0.97 mmol) was dispersed in 20 mL of deionized H_2O, and a few drops of HCl (33% by volume) were added. Addition of this solution to the NP suspension was carried out slowly (3 min) at room temperature, using a sonication bath for fast mixing and keeping continuous nitrogen bubbling in the reaction vessel. After 10 min, an external magnet was used to collect the magnetic product (FeNPs, 110 mg recovered), which contained the isonicotinic acid molecule as NPs shell and the Fe_3O_4 material for the core. Atomic absorption spectroscopy (AAS) analyses: 12 mg of dried FeNPs was digested with 10 mL of HCl (33%) and HNO_3 (1 mL, 6 N) until complete dissolution had been achieved and then diluted to 1 L with deionized water. Fe found, 8.60 ppm; Fe expected, 8.69 ppm.

Synthesis of the MM Complex, $[Ni(en)_2]_3[Fe(CN)_6]_2 \cdot 3H_2O$. Compound MM was prepared as previously reported.[37] In brief, solutions of 0.312 g (0.9 mmol) of $[Ni(en)_3]Cl_2 \cdot 2H_2O$ in 150 mL of H_2O and 0.198 g (0.6 mmol) of $K_3[Fe(CN)_6]$ in 150 mL of H_2O were prepared. The two solutions were mixed together and stirred for 2 min at room temperature. The resulting mixture was divided into two portions (portion (1) and portion (2), 150 mL each). The first portion (1) was left standing for only 1 day, affording the formation of nanocubes/nanospheres of MM as monitored through scanning electron microscopy (SEM). To this solution was added 5 mL of EtOH. Then the mixture was centrifuged at 4000 rpm (10 min), and the complex was recovered, washed with water, and dried (0.100 g). The second portion (2) was left standing for 1 week, over which time microcrystals of MM formed fully. The solid material was separated on a sintered funnel, washed with water, ethanol, and methanol, and dried in air (0.240 g). The chemical identities of MM in preparations (1) and (2) were found to be consistent with each other and agreed with the elemental analyses, magnetic properties, and IR fingerprints previously reported for the title compound. Anal. Calcd for $C_{24}H_{54}N_{24}O_3Fe_2Ni_3$: C, 28.41; H, 5.36; N, 33.13. Found: C, 28.45; H, 5.63; N, 33.02. AAS analyses: 8 mg of MM was digested with HCl (10 mL, 33%) and HNO_3 (2 mL, 6 N) until complete dissolution had been achieved and then diluted to 0.1 L with deionized water. Fe found, 8.73 ppm; Fe expected, 8.81 ppm.

Synthesis of the Hybrid Material. Suspensions of FeNPs (50 mg) in EtOH (20 mL) and MM nanocubes/nanospeheres (50 mg) in H_2O (deionized, 20 mL) were mixed together using two cycles of sonication (20 min) in a water bath at 50 °C. From one cycle to the other, 2 min of ageing was applied at the same temperature. Then the resulting mixture was left standing for 1 day at room temperature. The hybrid material was recovered from the mother solution with the use of an external magnet, washed twice with deionized water, and dried in a vacuum (85 mg). AAS analyses: 9 mg of hybrid material was digested with HCl (33%, 12 mL) and HNO_3 (1 mL, 6 N) until complete dissolution had been achieved and then diluted to 0.5 L with deionized water. Fe found, 7.44 ppm; the Fe expected for the 1:1 mixture of FeNPs and MM is 7.51 ppm.

Characterization Techniques. SEM images and energy-dispersive X-ray (EDX) spectroscopy data were recorded on a Hitachi 6600 FEG microscope. Dried powder samples were placed on an aluminum holder with double-sided adhesive carbon tape. The accelerating voltages used were in the range of 5–15 keV. The transmission electron microscopy (TEM) images and selected area electron diffractions (SAED) were taken on a JEOL 2010 microscope operating at 200 kV with a point-to-point resolution of 1.9 Å. Before measurements, aqueous suspensions of the materials were treated in an ultrasound bath at room temperature for 1–2 min. Drops of the dilute suspensions were placed onto a holey carbon film supported by a copper mesh TEM grid and air-dried at room temperature. The X-ray powder diffraction (XRD) patterns of all solid samples were recorded on an X'Pert PRO (PANalytical) instrument in Bragg–Brentano geometry with iron-filtered Co Kα radiation (40 kV, 30 mA, λ = 0.178901 nm) equipped with an X'Celerator detector and programmable divergence and diffracted beam antiscatter slits. The transmission ^{57}Fe Mössbauer spectra were measured using a Mössbauer spectrometer in a constant acceleration mode with the ^{57}Co(Rh) source. The isomer shift values were related to α-Fe at room temperature. The measurements were carried out in a closed helium cycle device at a temperature of 298 K with and without the application of an external magnetic field oriented parallel with respect to the propagation of γ-rays. Great care was taken to prepare the samples for Mössbauer spectroscopy with a uniform amount and thickness. The acquired Mössbauer spectra were fitted with the MossWinn software package. Prior to fitting, the signal-to-noise ratio was enhanced by a statistically based algorithm developed by Prochazka et al.[38] A superconducting quantum interference device MPMS XL-7 (Quantum Design) magnetometer was employed for the bulk magnetic measurements. The hysteresis loops were collected at different temperatures in external magnetic fields ranging from −70 to +70 kOe. The zero-field-cooled (ZFC) magnetization curves were recorded as the solution was warmed after it had been cooled in a zero magnetic field, while the field-cooled (FC) magnetization curves were recorded as the solution was cooled in external magnetic fields in the temperature range from 2 to 300 K. Fourier transform infrared (FT-IR) spectra of the dried samples were recorded on a Nexus 670 FTIR spectrometer (Thermo Nicolet) using a Smart Orbit diamond ATR technique (400–3950 cm^{-1}). The total amounts (in ppm, mg/L) of iron cations present in the samples (FeNPs, MM, and in the hybrid

dx.doi.org/10.1021/ic4008729 | Inorg. Chem. 2013, 52, 8144–8150

material) were determined by AAS with flame ionization using the Perkin-Elmer 3300 device (Perkin-Elmer). The samples for analyses were obtained by mixing a few milligrams of the solids with concentrated HCl and HNO_3/water solutions (6 M) followed by their digestion for 20 min at room temperature. Then these solutions were appropriately diluted with deionized water before the spectroscopic measurements. For determination of the Fe content we used the absorption line at 248.3 nm.

RESULTS AND DISCUSSION

The Self-Assembly Process of FeNPs and MM in Solution. The MM complex, $[Ni(en)_2]_3[Fe(CN)_6]_2{\cdot}3H_2O$, was selected in this study as the FeNPs partner because it exhibits different magnetic behaviors, such as field-induced antiferromagnetic−ferromagnetic−paramagnetic transitions with a Néel temperature (T_N) of ∼12 K and a critical field (H_C) of 11 kOe at T = 2 K.[37] In view of these properties, MM could potentially act as a probe for the local FeNPs' field and could conversely work as an antiferromagnetic (AF) or ferromagnetic (F) phase for the iron oxide nanoparticles, depending on temperature and the mutual strengths of the FeNPs−MM magnetic interactions. In order to prevent chemical reactions, for example, formation of covalent bonds between FeNPs and MM, and to promote effective assembly, the magnetite nanoparticles were surface functionalized with an organic molecule, isonicotinic acid, which was found to be chemically inert toward MM and exhibited high affinity for and stability toward the magnetite nanoparticles. The magnetic nanoparticles were obtained from magnetotactic bacteria, grown, and purified as described earlier (40 ± 5 nm mean size).[36,39] The FeNPs surface functionalization was achieved easily by reacting isonicotinic acid and magnetite at room temperature (T = 298 K, 10 min) in a nitrogen-saturated water medium without promoting surface degradation (e.g., due to the formation of FeO layers at the water−particle interface). The so-formed functionalized FeNP system retained a nearly spherical shape (Figure 2a, TEM image) and excellent Fe_3O_4 crystallinity (Figure S1, Supporting Information). The proclivity of FeNPs to self-assemble into hollow micrometer-sized (μm-sized) superstructures in water as well as in H_2O/EtOH solutions is shown in the SEM image of Figure 2b. This structural aspect constitutes the morphological signature of FeNPs adopted in this solvent(s) mixture. The use of in situ EDX analyses showed the expected elemental composition of FeNPs in these aggregates (Figure S2, Supporting Information). The complex MM was synthesized as reported previously,[37] by reacting $[Ni(en)_3]Cl_2{\cdot}2H_2O$ (1.5 equiv) with $K_3[Fe(CN)_6]$ (1 equiv) in water. The formation of small nanocubes/nanospheres of MM occurred after 1 day of reaction in dilute solution without external stirring (Figure 2c). Scanning electron microscopy combined with energy-dispersive X-ray (SEM-EDX) analyses of these intermediate nanostructures confirmed the expected composition of the material; furthermore, the elemental analyses revealed its hydrated form (SEM-EDX in Figure S3, X-ray diffraction pattern and Fourier transform infrared spectrum in Figure S1, Supporting Information). When MM was left standing in solution longer, large islands of crystalline material grew from the initial nanostructures, reaching the dimension of well-defined, μm-sized crystalline objects after 1 week at room temperature (Figure 2d). This feature corresponds to the morphological fingerprint of MM at the end of its crystallization process in solution if present in the system as a single component. The sonochemically assisted assembly of the hybrid material was achieved by adding together FeNPs in EtOH and MM nanocubes/nanospheres in water in a 1:1 ratio (weight), resulting in a morphologically new system. Assembly consisted of two sonication cycles (for 20 min at 50 °C) in a water bath followed by 1 day of standing in solution without stirring. The hybrid material formed in large cubic and spheroidal μm-sized superstructures that were separated from the solution (EtOH/H_2O) with the use of an external magnet (SEM micrographs in Figure 2e−h and Figure S4 in Supporting Information). These magnetic objects did not evolve back into separated phases of MM and FeNPs, namely, into μm-sized crystals of MM and large spherical aggregates of FeNPs, upon ageing longer in solution. Therefore, the hybrid system cannot be regarded as a simple admixture of the two distinct building units, MM and FeNPs, but consisted of new entities that

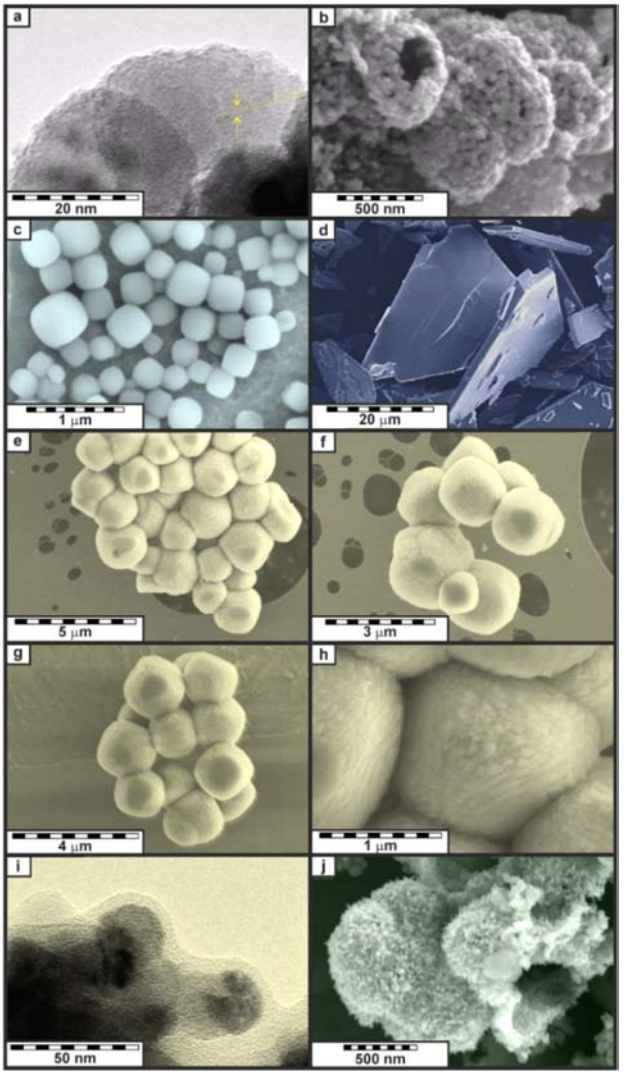

Figure 2. (a) TEM micrograph of FeNPs with crystalline lattice fringes (diffraction peak 311) highlighted by arrows. (b) SEM micrograph showing the spheroidal hollow superstructures of FeNPs. (c) SEM micrograph of MM nanocubes/nanospheres. (d) SEM micrograph of MM in the fully grown crystalline form. (e−h) SEM micrographs of the hybrid material. (i) TEM micrograph showing the layer of MM on the surface of FeNPs. (j) SEM micrograph of hybrid formed in the primary sonication stage while keeping the morphology of FeNPs (compare with panel b).

dx.doi.org/10.1021/ic4008729 | Inorg. Chem. 2013, 52, 8144−8150

created more complex superstructures without alteration of the chemical identity or composition of these two components (Figure S1, Supporting Information). In particular, during sonication, the nanocubes/nanospheres of MM fractionated into a continuous metallorganic matrix, covering and filling the hollow FeNPs superstructures (TEM micrograph in Figure 2i and SEM micrographs in Figure 2j and Figure S5 in Supporting Information). We found that the protracted sonication of MM and FeNPs for at least 20 min was required for the effective formation of the hybrid system. When FeNPs in EtOH and MM nanocubes/nanospheres in water were mixed together in the 1:1 ratio and subjected to either (i) a shorter sonication cycle (about 10 min at 50 °C) or (ii) mechanical stirring for 60 min (50 °C) followed by ageing in solution for 1 week, we observed that the hybrid material was poorly formed in the first case or completely absent in the latter case (Figures S6 and S7, Supporting Information).

The last scenario exactly reproduces what can be alternatively obtained by suspending directly large preformed crystals of MM and FeNPs in water using the 1:1 ratio, stirring the mixture for a few minutes, and collecting the two self-assembled components with the use of an external magnet (termed hereafter FeNPs/MM, see Supporting Information). Therefore, the prerequisites for formation of the soft−hard hybrid system were a subtle combination of the following factors: (i) an early stage in the crystallization process of MM toward building up much larger crystalline islands, (ii) the stability of the isonicotinic acid coating in FeNPs toward the neutral MM form and the resulting weak electrostatic interactions between the two components in solution, and (iii) the extended sonication time, which softened MM in such a way so as to initiate the FeNP covering process, filling the voids among the FeNP superstructures without the occurrence of chemical reactions with the FeNP surfaces. Therefore, MM acted as mortar for the FeNPs bricks, leading to the formation of μm-sized cubes/spheres. The bulk magnetic susceptibility measurements and Mössbauer spectroscopy were then used as tools to reveal the magnetic and electronic fingerprints of the hybrid system in comparison to those originally measured for the pure FeNPs and MM phases.

Magnetic Regime of the Hybrid Composite Compared to Those of FeNPs and MM as Isolated Systems. The bulk magnetic properties of surface functionalized FeNPs, MM, and the self-assembled product (hybrid) were probed at 300 K (Figure 3a) and 2 K (Figure 3b). At 300 K, the functionalized FeNPs phase exhibited high saturation magnetization (M_{sat} = 66.1 emu/g) and a small coercive field ($H_C \approx$ 120 Oe). These values increased slightly upon lowering the temperature to 2 K (M_{sat} = 72.5 emu/g and $H_C \approx$ 200 Oe). The temperature dependences of the ZFC and FC magnetization were characteristic of well-defined crystalline materials (Figure S8, Supporting Information), showing the presence of the Verwey transition around 120 K,[40,41] confirming that the surface functionalization with layers of isonicotinic acid did not alter the electronic signature of the Fe_3O_4 cores. The magnetic properties and saturation behavior of MM in the two morphologically distinct forms, nanoparticles (Figure 2c) and μm-sized crystals (Figure 2d), were found to be identical to each other. The saturation trend of MM at 300 K strictly followed that expected for simple paramagnetic species. The bulk magnetization was found to be linearly dependent on the applied magnetic field and exhibited a small saturation value of magnetization, falling at 1.1 emu/g (at 70 kOe, Figure 3a, green

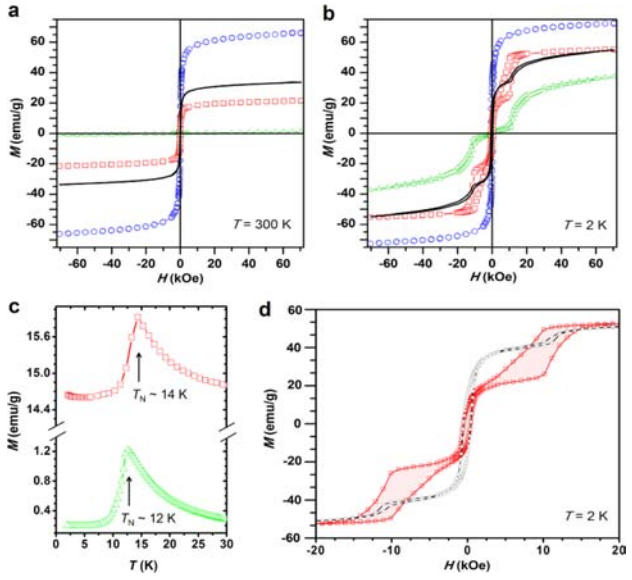

Figure 3. Magnetic hysteresis curves at T = 300 K (a) and T = 2 K (b) for FeNPs (blue circles), the molecular metamagnet MM (green triangles), their theoretical arithmetic average (1:1) of noninteracting particles (black line), and the hybrid material (red squares). Panel c shows the field-cooled (FC) magnetization trends for MM (green triangles) and the hybrid system (red squares) measured at 1 kOe. (d) Enlarged view of the magnetic hysteresis curves at T = 2 K of the hybrid system (red squares) and FeNPs/MM (1:1 ratio, gray circles).

triangles). The pure MM phase contains ferromagnetic interactions along the Ni/Fe chains and antiferromagnetic interactions active among neighboring chains, with magnetic ordering below 12 K (Figure 3c, green triangles). In the case of the hybrid system (Figure 3a, red squares), a lower value for the saturation magnetization was observed (21.6 emu/g at 300 K), a value much smaller by far than the one theoretically expected for the simple 1:1 admixture of two noninteracting spin active constituents (estimated $M_{sat} \sim$ 33.6 emu/g, Figure 3a, black line). In fact, the 1:1 mixture of FeNPs and MM prepared by simple mechanical stirring of the two components without sonication exhibited a M_{sat} value only slightly higher than the one expected from the 1:1 average (37.5 emu/g, FeNPs/MM, Figure S12 in Supporting Information). At room temperature, the hybrid system showed a coercivity of ∼200 Oe, a value larger than that observed for the Fe_3O_4 nanoparticles (∼120 Oe) or MM (0 Oe) probed as isolated components or in the mixed FeNPs/MM (∼130 Oe). Thus, the witnessed modification in coercivity for the hybrid material indicates the occurrence of large magnetic anisotropy. Three scenarios are proposed to explain the coercivity enhancement: (i) establishment of a magnetic ordering in MM, (ii) evolution of new easy axes of magnetization in the surface layers of FeNPs being in close contact with MM, and (iii) a combination of these two phenomena. Both saturation magnetization and coercivity values confirm the emergence of a magnetic interaction between the two counterparts in the hybrid that is stronger than that present in the simple admixture FeNPs/MM. The M_{sat} profile recorded for the hybrid material at different temperatures (300, 30, 14, and 2 K) increased with a decrease in temperature, and these additional plots are given in Figure S9 in Supporting Information. In particular, at 2 K, the observed M_{sat} value became as large as 55.3 emu/g (at 70 kOe) in the hybrid (Figure 3b, red squares). This value agrees

dx.doi.org/10.1021/ic4008729 | Inorg. Chem. 2013, 52, 8144−8150

surprisingly well with the averaged moment calculated for the 1:1 mixture, M_{sat} = (72.5 + 37.4)/2 = 55.0 emu/g (Figure 3b, black line). The witnessed effect seems to indicate that at higher applied magnetic fields the interaction between FeNPs and MM competes with field-induced ferromagnetic ordering in MM, and as such the external field is not sufficient to generate new, significant easy axes of magnetization in MM. However, T_N of MM in the hybrid system slightly increased from ∼12 to ∼14 K (Figure 3c, Figure S10 in Supporting Information), and the antiferromagnetic−ferromagnetic transition for MM shifted from 11 to 9.1 kOe (Figure S11, Supporting Information). The same T_N shift was observed in FeNPs/MM (Figure S12, Supporting Information). However, in the hybrid material, the ferromagnetic phase of MM origin showed a hysteretic behavior much stronger and more abrupt compared to that observed in MM alone or in the FeNPs/MM simple admixture (Figure 3d, gray circles). Furthermore, the coercivity of the hybrid (∼500 Oe) was found to be higher than that witnessed in FeNPs and MM but similar to that of FeNPs/MM at 2 K. Thus, the variation of the magnetic anisotropy is clearly linked to the extent of magnetic interaction between the two components, FeNPs and MM. From these data, it has been further concluded that in the hybrid system a more complex interplay between ferromagnetic exchange interactions of the layered material of MM in closer contact with FeNPs coexisted with the antiferromagnetic interactions within the MM material lying more distant from the FeNPs, even at room temperature. Both phenomena must overlap in a fraction of MM where the metamagnetic behavior is altered but not entirely modified; the presence of only one T_N at low temperature in the hybrid and FeNPs/MM mirrored, in fact, the existence of the aforementioned "less-perturbed" fraction of MM, namely the fraction left in the organometallic matrix as nonordered phase, being ordered below 14 K. While the magnetization and TEM/SEM measurements described so far brought unambiguous evidence for the formation of a novel system in the hybrid morphologically distinct from the simple admixture of FeNPs/MM and indicated larger magnetic anisotropy, the observed magnetic trends do not allow clear discrimination of the magnetic contributions of the soft and hard constituents. Therefore, we employed zero-field and in-field ^{57}Fe Mössbauer spectroscopy to gain further details of the complex magnetic interactions emerging from MM and FeNPs in the hybrid.

Mössbauer Spectroscopy. ^{57}Fe Mössbauer spectroscopy provides information on physical phenomena at a local level with a superior ability to discern the magnetic regimes of both counterparts. Here, the ^{57}Fe nucleus acts as a probe that screens the physical characteristics of its surroundings via hyperfine interactions.[42] The zero-field and in-field Mössbauer spectra of the hybrid sample, recorded at room temperature, are shown in Figure 4, and the derived values of the Mössbauer hyperfine parameters are listed in Table S1 in Supporting Information. In the case of FeNPs, the magnetic core is formed by Fe_3O_4 having a spinel structure. Two sextet components are expected to emerge in the zero-field Mössbauer spectrum at room temperature: one sextet originates from the Fe(III) cations occupying the tetrahedral sites and the other reflects the presence of Fe(II, III) cations lying at the octahedral sites. The molecular magnet MM behaves as a paramagnetic species at room temperature, with a doublet low-spin Fe(III) component clearly observable in its Mössbauer spectrum when MM is probed as pure single phase material (Figure S13, Supporting Information). Thus, the corresponding Mössbauer spectrum of

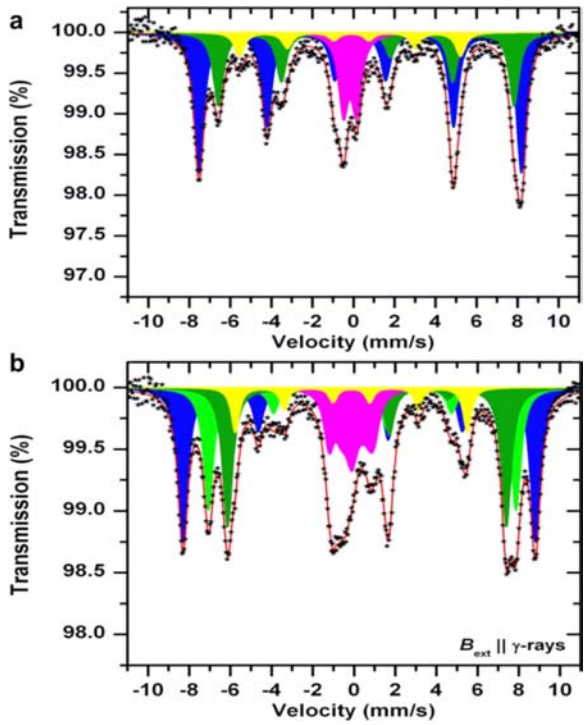

Figure 4. (a) Zero-field Mössbauer spectrum of the hybrid material recorded at 290 K. Spectrum components: S1 (blue), S2 (dark green), D (magenta), and S3 (yellow). (b) In-field Mössbauer spectrum (50 kOe) of the hybrid material recorded at 290 K. Spectrum components: S1 (blue) and S2 (dark green) have the same origin as in panel a; S3 (light green), S4 (magenta), and S5 (yellow). The symbols (★) represent experimental data, and the red line represents the spectrum fitting.

the hybrid system would be comprised of overlapped signals of three distinct components if no interaction occurred between MM and FeNPs. However, four spectral components were observed in the hybrid system (Figure 4a). Component S1 (blue) corresponds to the iron ions that occupy the tetrahedral positions in the Fe_3O_4 crystal structure, component S2 (dark green) to the iron ions lying in the octahedral positions in the Fe_3O_4 crystal structure, component D (magenta) to the paramagnetic iron ions in MM, and component S3 (yellow) to the iron ions from MM that are magnetically ordered because of the internal magnetic field of Fe_3O_4. The isomer shift value of this extra sextet (−0.15 mm/s) demonstrated that it originates from MM. Thus, MM as part of the hard−soft hybrid superstructure contributed the two components D and S3 to the overall spectral profile, and one of them reflected the presence of a magnetically ordered phase. This phase belongs to part of MM placed in close proximity to FeNPs in the framework of the hybrid. The witnessed effects underline the presence of an interaction mechanism active between FeNPs and MM in which FeNPs worked as a driving field strong enough to induce magnetization of some formerly paramagnetic MM layers. The observation of a local magnetic field in MM triggered by FeNPs is remarkable and unprecedented in materials chemistry because MM in pure phase is paramagnetic at room temperature. Notably, such interaction was found to be not only unidirectional but also mutual, as confirmed by in-field room-temperature Mössbauer analyses (Figure 4b). Because of the presence of the external magnetic field, the resonant lines were further split, revealing

dx.doi.org/10.1021/ic4008729 | Inorg. Chem. 2013, 52, 8144−8150

other sextet components with Mössbauer hyperfine parameter values that can be reconciled to the iron centers belonging to the Fe_3O_4 cores. From the fitting analyses, component S1 (blue) and component S2 (dark green) have the same origin as those shown previously in Figure 4a. Component S3 (light green) corresponds to the iron atomic positions at the surface layers of Fe_3O_4 nanoparticles affecting and being affected by interaction with MM, component S4 (magenta) to the iron ions in MM, and component S5 (yellow) to the iron ions from MM affected by the internal magnetic field of Fe_3O_4. The observed S5 component represents a fraction of iron cations involved in the interaction mechanism, a component that was previously hidden in the zero-field spectrum. The explanation of such an effect is linked to the Mössbauer hyperfine parameter values of S5 (especially the isomer shift and hyperfine magnetic field) that are falling "between" those of the Fe_3O_4 tetrahedral and octahedral spectral components. In addition, from the analyses of the in-field Mössbauer spectrum, it became possible to quantify the relative amount of iron cations on FeNPs and MM involved in the interaction process. Under the hypothesis that nonaffected and interaction-affected iron cations possess the same recoilless free fraction in both FeNPs and MM, we calculated that about one-third of iron cations in both FeNPs and MM were involved in this interaction.

Moreover, the in-field Mössbauer spectrum showed that the interaction components induced ferromagnetic-like ordering in affected FeNPs and MM layers because reduced intensities of the second and fifth sextet lines were observed compared to those obtained without the external magnetic field. It is important to underline that when a magnetic material ordering in an antiferromagnetic manner (like MM) is subjected to the perturbation of an external magnetic field applied in the direction of γ-rays, the behavior of the second and fifth Mössbauer sextet lines either is opposite (namely, exhibiting a slight increase in intensities) when the characteristic switching field of the material is overcome or is mostly unchanged, as was witnessed here. Therefore, the decreased saturation magnetization observed for the hybrid system at room temperature, previously shown in Figure 3a, mirrors the increased magnetic anisotropy of the surface layers of MM being in closer contact with FeNPs, which does not permit straightforward orientation of the magnetic moments to an external magnetic field. Such an effect is evident from the nonvanishing contribution of the intensities in the second and fifth Mössbauer resonant lines for the S1, S2, S3, and S5 components witnessed in the in-field room-temperature Mössbauer spectrum when compared to the spectrum for bare FeNPs in which these lines are clearly missing. At very low temperature, below 14 K, when the MM counterpart is completely ordered, competition between antiferromagnetic ordering of the MM itself and ferromagnetic ordering of the affected MM layers seems to favor one type of arrangement over the other when an external magnetic field is applied. This competition was documented by the rather complex behavior of the hysteresis loop observed under external magnetic fields higher than 1 kOe (Figure 3d). Thus, from the analysis of the recorded Mössbauer spectra, the following key conclusions are drawn: (i) the internal magnetic field of FeNPs induced magnetization within affected atomic layers of the molecular magnet MM already at room temperature; (ii) the interaction mechanism was not unidirectional; and (iii) the magnetic arrangement was ferromagnetic in nature for the MM layers in closer contact with FeNPs.

CONCLUSIONS

In summary, we reported here the sonochemically-assisted self-assembly process of surface functionalized magnetite nanoparticles (FeNPs) and the metamagnetic nanocubes/nanospheres Fe/Ni complex (MM) that led to formation of a morphologically novel magnetic material. The hybrid material was characterized by μm-sized objects of various shapes and dimensions (cubes and spheres). In the hard−soft hybrid, MM acted as a continuous metallorganic matrix, surrounding and filling the hollow superstructures of the FeNPs. The local magnetic fields generated by the caged FeNPs were strong enough to alter significantly, even at room temperature, the paramagnetic behavior of layers of MM in closer contact to FeNPs, forcing MM to adopt the ferromagnetic state. This approach to the synthesis of complex systems may offer novel opportunities to develop alternative routes to envisioning self-assembly processes where magnetic nanoparticles would substitute for large external magnetic fields and thereby considerably change the properties of soft magnetic molecular counterparts. One promising extension of this synthetic approach could involve the admixture of magnetic nanoparticles with single-molecule magnets in order to test the effectiveness of an intrinsic magnetic field in tuning the blocking temperature T_b and height of the activation barrier for spin reversal of the soft metallorganic molecule.[43−50] Such attempts are currently in progress.

ASSOCIATED CONTENT

Supporting Information

XRD pattern and FT-IR spectra of hybrid material, MM, and FeNPs; SEM and TEM micrographs showing the formation of spheroidal aggregates of functionalized FeNPs; SEM-EDX spectrum of FeNPs; SEM micrographs showing the formation of nanocubes/nanospheres of MM after 1 day in solution and after 1 week, the various structural assemblies of the hybrid system, and the self-assembly progress of MM and FeNPs toward the hybrid system; SEM micrograph of the composite material obtained after a short sonication cycle; SEM micrographs of the composite material obtained without sonication cycle; ZFC and FC magnetization curves for FeNPs and hybrid material; FC magnetization trends for MM and the hybrid system at different magnetic fields; virgin curves of magnetization for MM and hybrid material; temperature dependence of M_{sat} for the hybrid, FC magnetization curves at different fields for FeNPs/MM; room-temperature Mössbauer spectrum of MM; Mössbauer parameters derived from the zero-field and in-field Mössbauer spectra of the hybrid material. This material is available free of charge via the Internet at http://pubs.acs.org.

AUTHOR INFORMATION

Corresponding Author

*E-mail: radek.zboril@upol.cz.

Notes

The authors declare no competing financial interest.

ACKNOWLEDGMENTS

The authors acknowledge the support of the Operational Program Research and Development for Innovations−European Regional Development Fund (CZ.1.05/2.1.00/03.0058 from the Ministry of Education, Youth and Sports of the Czech Republic), Operational Program Education for Competitive-

ness−European Social Fund (CZ.1.07/2.3.00/20.0017 from the Ministry of Education, Youth and Sports of the Czech Republic), and of the Czech Science Foundation (P208/12/G016 and P207/11/0841).

REFERENCES

(1) Cornell, R. M.; Schwertmann, U. *The Iron Oxides: Structures, Properties, Reactions, Occurrences and Uses*; Wiley-VCH: Weinheim, Germany, 2003.
(2) Laurent, S.; Forge, D.; Port, M.; Roch, A.; Robic, C.; Elst, L. V.; Muller, R. N. *Chem. Rev.* **2008**, *108*, 2064−2110.
(3) Pan, Y.; Du, X.; Zhao, F.; Xu, B. *Chem. Soc. Rev.* **2012**, *41*, 2912−2942.
(4) Pan, Y.; Long, M. J. C.; Lin, H.-C.; Hedstrom, L.; Xu, B. *Chem. Sci.* **2012**, *3*, 3495−3499.
(5) Wilkinson, K.; Ekstrand-Hammarström, B.; Ahlinder, L.; Guldevall, K.; Pazik, R.; Kępiński, L.; Kvashnina, K. O.; Butorin, S. M.; Brismar, H.; Önfelt, B.; Österlund, L.; Seisenbaeva, G. A.; Kessler, V. G. *Nanoscale* **2012**, *4*, 7383−7393.
(6) Wei, Y.; Han, S.; Walker, D. A.; Warren, S. C.; Grzybowski, B. A. *Chem. Sci.* **2012**, *3*, 1090−1094.
(7) Wu, W.; He, Q.; Jiang, C. *Nanoscale Res. Lett.* **2008**, *3*, 397−415.
(8) Chaudhuri, R. G.; Paria, S. *Chem. Rev.* **2012**, *112*, 2373−2433.
(9) Frey, N. A.; Peng, S.; Cheng, K.; Sun, S. *Chem. Soc. Rev.* **2009**, *38*, 2532−2542.
(10) Lu, A.-H.; Salabas, E. L.; Schüth, F. *Angew. Chem., Int. Ed.* **2007**, *46*, 1222−1224.
(11) Zhou, J.; Meng, L.; Lu, Q.; Fu, J.; Huang, X. *Chem. Commun.* **2009**, 6370−6372.
(12) Prinz, A. G. *Science* **1998**, *282*, 1660−1663.
(13) Hwang, H. Y.; Iwasa, Y.; Kawasaki, M.; Keimer, B.; Nagosa, N.; Tokura, Y. *Nat. Mater.* **2012**, *11*, 103−113.
(14) Skumryev, V.; Stoyanov, S.; Zhang, Y.; Hadjipanayis, G.; Givord, D.; Nogués, J. *Nature* **2003**, *423*, 850−853.
(15) Paul, M.; Kufer, D.; Müller, A.; Brück, S.; Goering, E.; Kamp, M.; Verbeeck, J.; Tian, H.; Tendeloo, G. V.; Ingle, N. J. C.; Sing, M.; Claessen, R. *Appl. Phys. Lett.* **2011**, *98*, 012512.
(16) Sun, X.; Huls, N. F.; Sigdel, A.; Sun, S. *Nano Lett.* **2012**, *12*, 246−251.
(17) Namai, A.; Yoshikiyo, M.; Yamada, K.; Sakurai, S.; Goto, T.; Yoshida, T.; Miyazaki, T.; Nakajima, M.; Suemoto, T.; Tokoro, H.; Ohkoshi, S.-I. *Nat. Commun.* **2012**, *3*, 1035.
(18) Zheng, R. K.; Wen, G. H.; Fung, K. K.; Zhang, X. X. *Phys. Rev. B* **2004**, *69*, 214431.
(19) Ong, Q. K.; Lin, X.-M.; Wei, A. *J. Phys. Chem. C* **2011**, *115*, 2665−2672.
(20) Gupta, A. K.; Gupta, M. *Biomaterials* **2005**, *26*, 3995−4021.
(21) Atanasijevic, T.; Jasanoff, A. *Nat. Protoc.* **2007**, *2*, 2582−2589.
(22) Horcajada, P.; Chalati, T.; Serre, C.; Gillet, B.; Sebrie, C.; Baati, T.; Eubank, J. F.; Heurtaux, D.; Clayette, P.; Kreuz, C.; Chang, J.-S.; Hwang, Y. K.; Marsaud, V.; Bories, P.-N.; Cynober, L.; Gil, S.; Ferey, G.; Couvreur, P.; Gref, R. *Nat. Mater.* **2010**, *9*, 172−178.
(23) Cho, N.-H.; Cheong, T.-C.; Min, J. H.; Wu, J. H.; Lee, S. J.; Kim, D.; Yang, J.-S.; Kim, S.; Kim, Y. K.; Seong, S.-Y. *Nat. Nanotechnol.* **2011**, *6*, 675−682.
(24) Xie, J.; Liu, G.; Eden, H. S.; Ai, H.; Chen, X. *Acc. Chem. Res.* **2011**, *44*, 883−892.
(25) Fan, K.; Cao, C.; Pan, Y.; Lu, D.; Yang, D.; Feng, J.; Song, L.; Liang, M.; Yan, X. *Nat. Nanotechnol.* **2012**, *7*, 459−464.
(26) Cheng, Z.; Zaki, A. A.; Hui, J. Z.; Muzykantov, V. R.; Tsourkas, A. *Science* **2012**, *338*, 903−910.
(27) Bakandritsos, A.; Papagiannopoulos, A.; Anagnostou, E. N.; Avgoustakis, K.; Zboril, R.; Pispas, S.; Tucek, J.; Ryukhtin, V.; Bouropoulos, N.; Kolokithas-Ntoukas, A.; Steriotis, T. A.; Keiderling, U.; Winnefeld, F. *Small* **2012**, *8*, 2381−2393.
(28) Maity, D.; Zoppellaro, G.; Sedenkova, V.; Tucek, J.; Safarova, K.; Polakova, K.; Tomankova, K.; Diwoky, C.; Stollberger, R.; Machala, L.; Zboril, R. *Chem. Commun.* **2012**, *48*, 11398−11400.
(29) Zeng, H.; Li, J.; Liu, J. P.; Wang, Z. L.; Sun, S. *Nature* **2002**, *420*, 395−398.
(30) Coey, J. M. D. *Philos. Trans. R. Soc., A* **1998**, *356*, 1519−1541.
(31) Chen, G. F.; Li, Z.; Li, G.; Zhou, J.; Wu, D.; Dong, J.; Hu, W. Z.; Zheng, P.; Chen, Z. J.; Yuan, H. Q.; Singleton, J.; Luo, J. L.; Wang, N. L. *Phys. Rev. Lett.* **2008**, *101*, 057007.
(32) Serrate, D.; De Teresa, J. M.; Algarabel, P. A.; Fernández-Pacheco, R.; Galibert, J.; Ibarra, M. R. *J. Appl. Phys.* **2005**, *97*, 084317.
(33) Liu, X.; Panguluri, R. P.; Huang, Z.-F.; Nadgorny, B. *Phys. Rev. Lett.* **2010**, *104*, 035701.
(34) Morales, J. R.; Tanju, S.; Beyermann, W. P.; Garay, J. E. *Appl. Phys. Lett.* **2010**, *96*, 013102.
(35) State, H. M.; Reid, I. K.; Dwyer, F. P. In *Inorganic Syntheses*; Rochow, E. G., Ed.; McGraw-Hill: New York, 1960; Vol. *6*, pp 200−201.
(36) Markova, Z.; Siskova, K.; Filip, J.; Safarova, K.; Prucek, R.; Panacek, A.; Kolar, M.; Zboril, R. *Green Chem.* **2012**, *14*, 2550−2558.
(37) Herchel, R.; Tucek, J.; Travnicek, Z.; Petridis, D.; Zboril, R. *Inorg. Chem.* **2011**, *50*, 9153−9163.
(38) Prochazka, R.; Tucek, P.; Tucek, J.; Marek, J.; Mashlan, M.; Pechousek, J. *Meas. Sci. Technol.* **2010**, *21*, 025107.
(39) Markova, Z.; Bourlinos, A. B.; Safarova, K.; Polakova, K.; Tucek, J.; Medrik, I.; Siskova, K.; Petr, J.; Krysmann, M.; Giannelis, E. P.; Zboril, R. *J. Mater. Chem.* **2012**, *22*, 16219−16223.
(40) Verwey, E. J. *Nature* **1939**, *144*, 327−328.
(41) Lee, S.; Fursina, A.; Mayo, J. T.; Yavuz, C. T.; Colvin, V. L.; Sofin, R. G. S.; Shvets, I. V.; Natelson, D. *Nat. Mater.* **2008**, *7*, 130−133.
(42) Dormann, J. L.; Fiorani, D.; Tronc, E. In *Advances in Chemical Physics*; Prigogine, I., Rice, S. A., Eds.; John Wiley and Sons: New York; 1998; Vol. *98*, pp 283−494.
(43) Branzoli, F.; Carretta, P.; Filibian, M.; Zoppellaro, G.; Graf, M. J.; Galan-Mascaros, J.-R.; Fuhr, O.; Brink, S.; Ruben, M. *J. Am. Chem. Soc.* **2009**, *131*, 4387−4396.
(44) Chilton, N. F.; Langley, S. K.; Moubaraki, B.; Soncini, A.; Batten, S. R.; Murray, K. S. *Chem. Sci.* **2013**, *4*, 1719−1730.
(45) Zhu, Y.-Y.; Cui, C.; Zhang, Y.-Q.; Jia, J.-H.; Guo, X.; Gao, C.; Qian, K.; Jiang, S.-D.; Wang, B.-W.; Wang, Z.-M.; Gao, S. *Chem. Sci.* **2013**, *4*, 1802−1806.
(46) Branzoli, F.; Carretta, P.; Filibian, M.; Graf, M. J.; Klyatskaya, S.; Ruben, M.; Coneri, F.; Dhakal, P. *Phys. Rev. B* **2010**, *13*, 134401.
(47) Sessoli, R.; Powell, A. K. *Coord. Chem. Rev.* **2009**, *253*, 2328−2341.
(48) Car, P.-E.; Perfetti, M.; Mannini, M.; Favre, A.; Caneschi, A.; Sessoli, R. *Chem. Commun.* **2011**, *47*, 3751−3753.
(49) Sessoli, R.; Tsai, H.-L.; Schake, A. R.; Wang, S.; Vincent, J. B.; Folting, K.; Gatteschi, D.; Christou, G.; Hendrickson, D. N. *J. Am. Chem. Soc.* **1993**, *115*, 1804−1816.
(50) Ruamps, R.; Maurice, R.; Batchelor, L.; Boggio-Pasqua, M.; Guillot, R.; Barra, A. L.; Liu, J.; Bendeif, E.-E.; Pillet, S.; Hill, S.; Mallah, T.; Guihéry, N. *J. Am. Chem. Soc.* **2013**, *135*, 3017−3026.